X-Ray Diffraction (XRD) Characterization of Microstrain in Some Iron and Uranium Alloys

G. Kimmel, D. Dayan, G. A. Frank and A. Landau

1. Summary

The high linear attenuation coefficient of steel, uranium and uranium based alloys is associated with the small penetration depth of X-rays with the usual wavelength used for diffraction. Nevertheless, by using the proper surface preparation technique, it is possible of obtaining surfaces with bulk properties (free of residual mechanical microstrain). Taking advantage of the feasibility to obtain well prepared surfaces, extensive work has been conducted in studying XRD line broadening effects from flat polycrystalline samples of steel, uranium and uranium alloys.

The XRD line broadening analysis has been used as a semi- quantitative method for measuring nonhomogeneity of alloying, hardness, Izod notch toughness, fracture toughness and residual thermal stresses. Good correlation between the microstrain and properties such as hardness and toughness was found after heat treatments and cold work. Comparable correlation was found between the microstrain in the supersaturated α-uranium phase quenched from the γ region, and the concentration of the alloying elements. The measured microstrain in the supersaturated α-uranium phase was used as a quantitative indicator for determination of the solubility limit of Ta and W in γ-uranium.

2. Introduction

X-ray diffraction (XRD) is a valuable technique that can yield considerable information on structure and properties of crystalline materials. This technique not only identifies the phases present in a sample but can provide more information from the peak profiles, allowing determination of crystallite size and microstrain, on the structure of crystalline phases.

For perfectly periodic ideal crystals the intensity profile can be described as shock spikes placed at the solutions of Bragg's equation:

$$\lambda=2d\sin\theta \qquad (1)$$

Where λ is the X-ray wave length , d is the interplanar spacing (d-spacing) and θ is the scattering angle (Bragg's angle).

For *real* polycrystalline materials the intensity profile tends to be broader due to two main imperfections: Scattering from small coherent domains (Scherrer, 1918), and internal microstrain associated with variations in the d-spacing of the scattering crystals (Stokes and Wilson, 1944).

The experimental intensity profile can be regarded as a convolution of two profiles. The first is from a *real* polycrystalline sample and the latter is due to non-ideal experimental conditions. The letter is known as the *instrumental profile* and its broadening arises from factors such as, axial divergence, flatness, transparency and surface roughness of the sample (Wilson, 1962).

In order to extract the *real* crystal profile from the total broadening, it is necessary to deconvolute the instrumental broadening from the experimental profile. The full width at half maximum (FWHM) is used as a measure of the total broadening in this work. By performing *line profile fitting* to the experimental diffraction results, the FWHM is evaluated for every diffraction peak . Fitting the best polynomials (in this case second order) to the sample's and to a reference samples FWHMs as a function of θ gives a continuous representation of the experimental $B(\theta)$ and instrumental $b(\theta)$ broadening, respectively. The deconvolution of $b(\theta)$ from $B(\theta)$, i.e., the calculation of the broadening coming from the real crystals $\beta(\theta)$, can be obtained by one of the following equations:

$$\beta(\theta)^2=B(\theta)^2-b(\theta)^2 \qquad (2a)$$

$$\beta(\theta)=B(\theta)-b(\theta) \qquad (2b)$$

Equations 2a and 2b assume Gaussian and Lorentzian forms of diffraction peaks, respectively. This assumption is rarely true and has to be regarded as an approximation. In cases where most of the experimental broadening arises from the sample, i.e., $B(\theta)^2>>b(\theta)^2$ both equations give good approximation for $\beta(\theta)$ (Klug and Alexander,1974). Only such cases will be considered in this work.

The strain ε and the coherent domain size L can be obtained by Klug-Alexander dependence:

$$\beta^2 cos^2(\theta)=(\lambda/L)^2+16\varepsilon^2 sin^2(\theta) \qquad (3a)$$

$$\beta cos(\theta)=(\lambda/L)+4\varepsilon sin(\theta) \qquad (3b)$$

This expression can be derived from Bragg's equation by assuming Gaussian or Lorentzian broadening functions for both strain and size. Although this assumption does not agree with the opinion that Gaussian and Lorentzian broadening arises from strain and size effects respectively (Halder and Wagner, 1966; Gupta and Anantharaman, 1971; Nandi and Sen Gupta, 1978), we used this dependence for two reasons: (i) in this work the strain effect is more dominant; and (ii) the strain and size are evaluated by linear regression of $\beta^2 cos(\theta)$ *vs* $sin^2(\theta)$ termed Williamson-Hall plot (Williamson and Hall, 1953; Langford, 1992). Therefore, if Klug-Alexander dependence is not a good approximation for the systems analyzed in this work these will be, poor linear correlation.

Due to the high attenuation factor of uranium and steels, the X-ray penetration depth is relatively small (2-5μm). Hence, the information obtained by XRD broadening analysis is relevant only to the surface. Thus, gaining information about the bulk by this method depends upon surface treatments that will erase surface damage resulting from polishing and grinding. Because mechanical polishing can introduce strains into the surface, other methods for peeling of damaged surface layers have to be used, leaving only the effects in the bulk material.

An enormous number of steels with different compositions and properties is used as one of the principal structural materials. The proper process needed to achieve the desired assets is well documented. The preferred commercial materials is those which tolerate deviation in process conditions without damaging the final quality.

However, the ability to maintain small tolerance of some characteristics with a wide range of production conditions is not always clear and the desired quality is not easy to attain, due to the poor sensitivity of the characteristic. For example, the density and the composition will not change significantly within a wide range of tempering conditions for certain steel. The correlation between XRD line width and the condition of steels is well known. In residual stress measurements the broadened diffraction lines of some steels are inconvenient and special care must be taken for the determination of line position (Kurita, 1991). Line broadening analysis is currently studied in plastically deformed metals and in ball milled iron powders (Wagner and Aqua, 1963; Ungár, 1995) in order to investigate unisotropical distribution of internal stresses. In the present work we studied XRD broadening effects in steels, in samples with different mechanical properties, in order to determine whether mechanical properties and XRD broadening are correlated.

Iron exhibits three solid phases before melting at ≈1540°C. The solid phases consist of the following crystallographic structures: δ(1400-1540°C) is cI2, i.e., tungsten type; γ(910-1400°C) is cF4, i.e., copper type; and α(below 910°C) is cI2 also, but with smaller lattice parameter.

Rapid cooling of steel from the γ-phase to the α can produce a highly distorted supersaturated phase with a *tI2* (body centered tetragonal) structure designated by α'. This phase is created by athermal martensitic transformation and gives rise to a hard and brittle product.

Uranium with a melting point of approximately 1132°C has three phases: γ (775-1132°C) is cubic-*cI2*; β(668-to 775°C) is complex *tP30*, i.e., primitive tetragonal with 30 atoms per unit cell and α (below 668°C) is orthorhombic-*cO4* (Burke & al., 1976). As determined by X-ray measurements, the γ→β and β→α transitions are accompanied by volume decreases of 0.70% and 1.12% respectively (Chiotti et al., 1959). Studies with pure uranium have shown that neither of the high temperature phases, γ or β could be retained by quenching. The addition of various solutes to uranium enables one to obtain the isothermal martensitic transformation β→α or the athermal transformation γ→α. The final product is generally supersaturated with the solute and slightly distorted. Those phenomena are related to the cooling rate and composition of the uranium base alloys. The U-Ta, U-W and U-V alloys belong to binary systems with low solubility in the γ-uranium; (Saller and Rough,1952). Schramm et al., 1950; Dayan et al., 1994; Kimmel and Dayan, 1995; Dayan and Kimmel, 1996. Rapid cooling from the γ-phase is accompanied by the formation of α'-phase. The high strength and hardness of the quenched samples and the nature of the broad diffraction patterns, indicate that a state of non-uniform microstress exists in the alloys (Douglas, 1961). After prolonged annealing at high α range, the broadening effects of γ quenched uranium alloys are suppressed due to complete segregation of the solute and other impurities.

In the present paper we report on XRD line broadening effects in pure uranium and in various uranium alloys caused by different heat treatments, alloying, cold work, and surface preparation techniques. We also show that line broadening analysis may become a sensitive tool for evaluation of Izod notch and fracture toughness in steels and in uranium alloys, respectively.

3. Experimental Techniques

3.1 General methodology

The XRD analysis was performed with a Philips diffractometer using monochromatic Cu-radiation (λ=0.15406 nm for the $K_{\alpha 1}$ characteristic line). The K_β was removed by a reflected beam graphite monochromator. X-ray data were taken from 20 to 150° 2θ, while scanning in steps of 0.02° (2θ) with counting intervals ranging from 0.5 to 8 sec per step. The multiline integral breadth method (Williamson and Hall, 1963) has been adopted for evaluation of the mean coherent cell size and the average microstrain. The Williamson-Hall procedure has the advantage of speed and convenience (Guillou et al., 1995), and it has been utilized in other recent studies such as Langford et al. (1993) and Louër (1994). A similar method was presented by Langford et al. (1986). Utilization of the more powerful Fourier (Warren-Averbach), variance and related methods was abandoned at this stage because most of the diffraction lines in uranium are not well resolved, due to the low symmetry of U-α structure. Moreover, in case we find an isolated line in the lower Bragg angles, such as *020* or *111*, the higher orders of these reflections are indistinct and too close to other lines. This limitation of the Warren-Averbach method has been mentioned in earlier

work (Langford et al., 1988). Nevertheless, utilization of the Fourier (WA) methods is investigated now.

The followings procedure have been used for the line profile analysis:

1. Selecting a range of the analyzed diffractograms with some diffraction peaks.
2. Performing line profile fitting for each peak that results in *FWHM of profile*, area, and height values for each Bragg line. This procedure is done with Philips PC-APD software, and gives a fixed *FWHM* to integral breadth ratio. In our software version the fitting is made in steps including no more than eight Bragg reflections at a time. A typical example of profile fitting results is shown in Fig. 1.

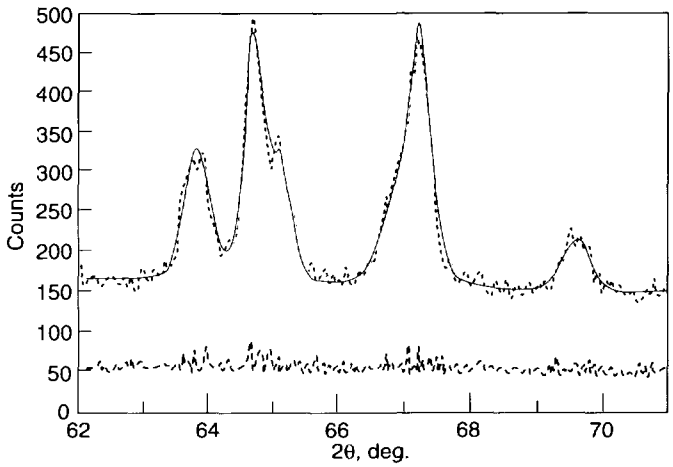

Fig. 1: An example of profile fitting for a selected XRD spectrum.

3. Finding the best fitted polynomial function $B(\theta)=a_0+a_1\theta+a_2\theta^2$ for the *FWHM* of the sample.
4. Finding the best fitted polynomial function $b(\theta)=a_0+a_1\theta+a_2\theta^2$ for the *FWHM* of the corundum plate standard (NIST, 1976), simulating the instrumental broadening.
5. The extent of the broadening effect can be examined visually just by looking at the vertical displacement of the B line, from the b line as seen in Fig.2 Then, by using equation 2a or 2b, the *real* sample broadening $b(\theta)$ can be extracted.

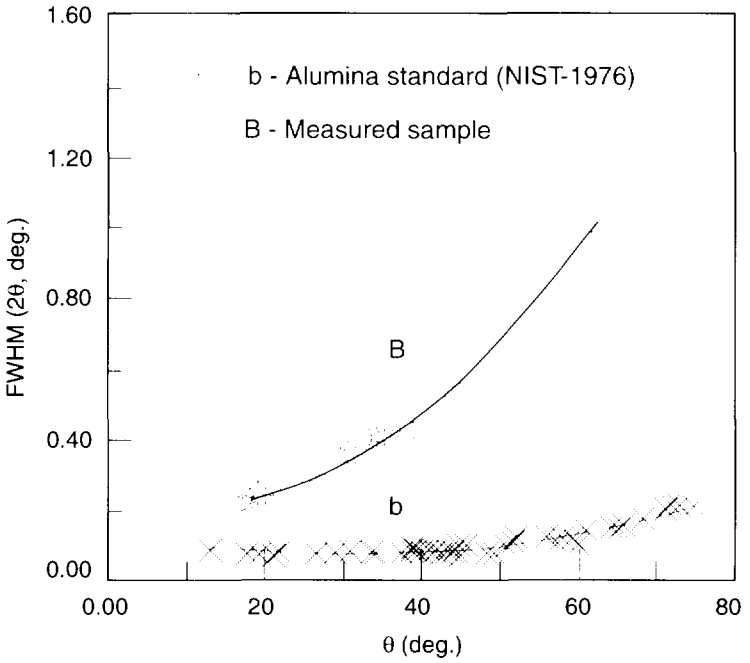

Fig. 2: Broadening effect: a comparison between B and b plots vs 2q. The function B(θ) is measured from the uranium spectrum and b(q) as obtained from corundum plate (NIST1976).

6. Strain and size data derived from the Williamson-Hall plot using eq. 3 for our application are shown in Fig.3 for uranium after cold work (forging).

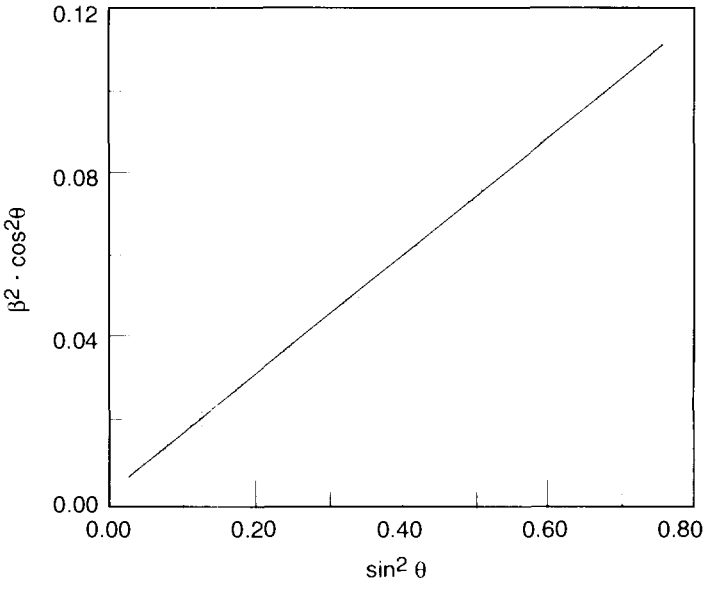

Fig. 3: Williamson-Hall plot for the case shown in Figure 2.

3.2 Samples preparation

Steels - The samples were prepared from several types of steels such as carbon-based alloyed steel, plain carbon steels and high-speed steel (HSS). All elemental concentrations are given in weight-percent. Different

toughness and hardness were obtained by different thermal treatment, which included quenching from the γ-phase and tempering. Most samples sliced from Izod test specimens were polished mechanically and then electrolytically to remove the surface damage.

Uranium and uranium alloys - Small ingots of pure uranium U- 0.2 wt% (0.93at.%)V, U-0.75wt%Ti, and dilute uranium tantalum and tungsten alloys were prepared in an arc melting furnace under an atmosphere of purified argon. The various cast samples were remelted several times and the alloys were heat-treated in a vacuum furnace at 1040°C for 24 h. to ensure reasonable homogeneity. Chemical analysis, microscopy (light and SEM-EDAX) and surface hardness were used for the structural, morphological and mechanical characterization. The characterization of the microstrain and coherent domain size in the different samples was evaluated from a line profile analysis of XRD spectra.

Several U-Ti samples were prepared for fracture toughness measurement. These samples were water-quenched from γ treatment (20 min. at 850°C), followed by aging at 370°C for 6 h. The fracture toughness test took place at -40°C.

Surface preparation - In order to establish whether it is possible to obtain reliable surfaces for XRD of steel, uranium and uranium alloys, we performed some measurements on mechanically and electrolytically polished surfaces of pure uranium and low alloyed steel. After each preparation stage, an XRD analysis was performed and the

breadths of the different peaks were measured and then plotted against theta in degrees.

Figure 4 shows diffractograms of tempered steel fully annealed after mechanical polishing. (3000 mesh diamond) and electrolytic polishing. The effect of the latter was marked; in all lines $K\alpha_1$- $K\alpha_2$ are split and the carbides lines are detected. Without electropolishing, $K\alpha_1$- $K\alpha_2$ are always overlapped and the carbides lines are hidden.

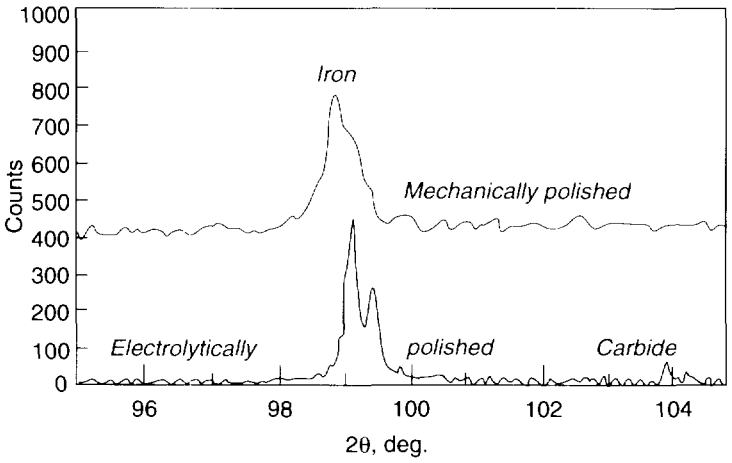

Fig. 4: Diffractograms of tempered steel as mechanically (top) and electrolytically (down) polished surface.

Figure 5 shows the FWHM versus θ plots for these two cases, in both of which there is uniform broadening. Williamson-Hall treatment results in a low level of microstrain (0.07%) and no size effect in the electropolished surface; and in microstrain of 0.165% and a domain size of 63 nm for the mechanically polished surface.

A flat surface of an annealed pure uranium sample was selected for the examination of surface treatment. The flat surface was examined by XRD after mechanical grinding with emery papers, polishing with diamond cloths, and finally after electropolishing in a bath containing 50 g of chromic acid, 420 cc of acetic acid and 60 cc of distilled

water.

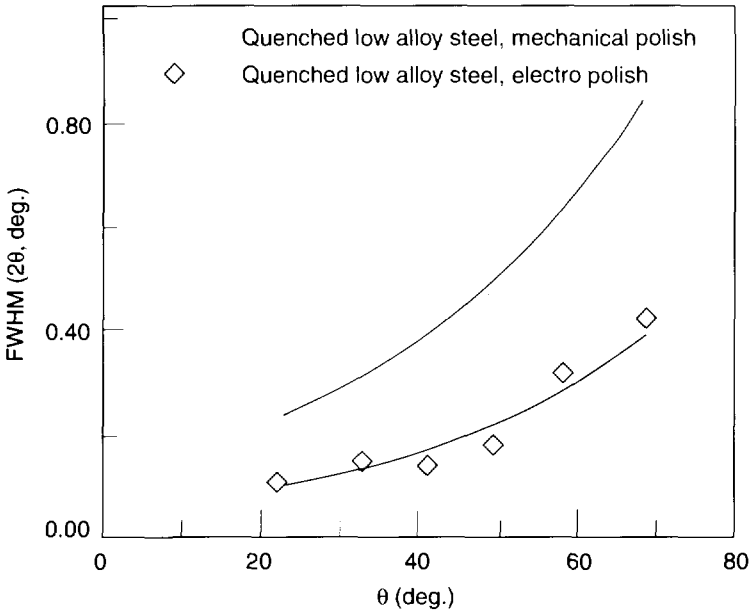

Fig. 5: Line breadth (FWHM) of quenched low alloy steel as mechanically (top) and electrolytically polished surface (down).

Figure 6 shows five plots of *FWHM* of XRD lines vs Bragg angle θ. The sample with mechanical grinding on 180 grit paper exhibited the broadest diffraction lines. Finer paper (1000 grit) resulted in similar broad XRD lines. Diamond polishing reduced the broadening effect, and electropolishing removed most broadening effects.

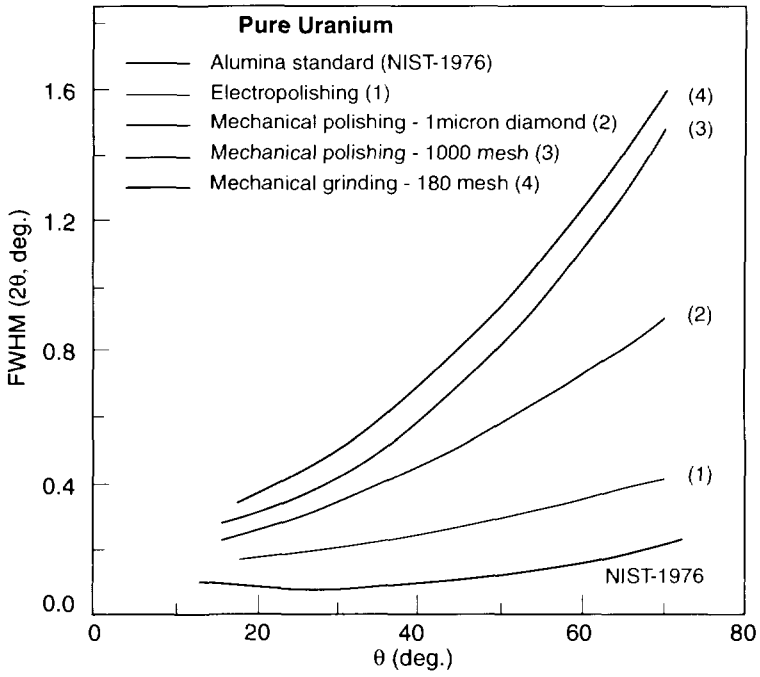

Fig. 6: Broadening effects in pure uranium with several degrees of surface damage.

Similar behaviors were obtained for U-0.2wt.%V after the same surface treatment. The results are illustrated via Williamson-Hall plots in Figure 7.

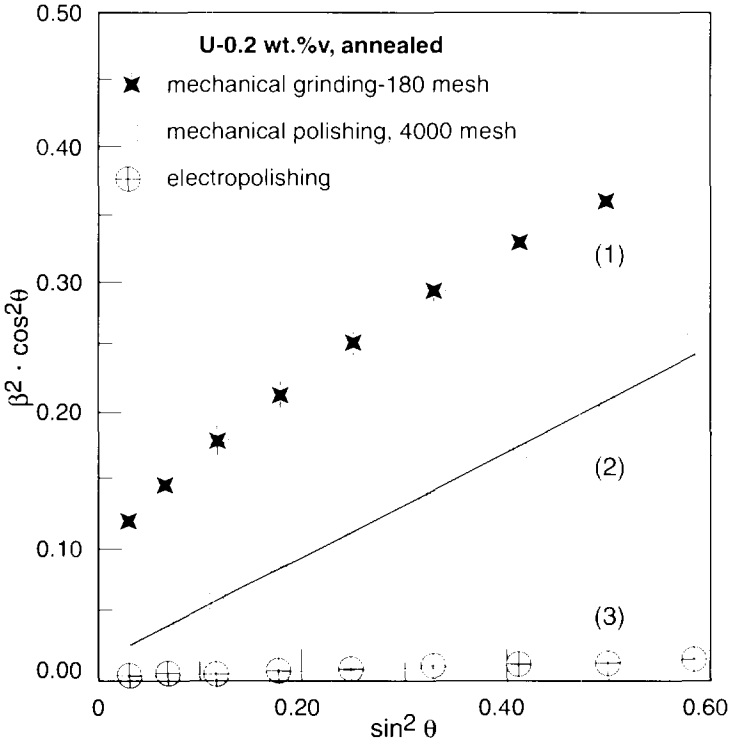

Fig. 7: Williamson-Hall plots for U - 0.2%wt V, after several degrees of surface damage (see also Table 1).

Table 1: Strain and size data for uranium surfaces

Sample	Surface treatment	Microstrain %	Mean coherent cell size nm
pure uranium	grinding, 180 mesh	0.331	31
pure uranium	polishing 4000 mesh	0.253	155
pure uranium	electropolishing	0.043	-
U - 0.2 wt.% V	grinding 180 mesh	0.312	26
U - 0.2 wt.% V	polishing 4000 mesh	0.260	150
U - 0.2 wt.% V	electropolishing	0.063	-

4. Results

4.1 Medium alloyed steel

We received from the industry several samples of 0.4% C, 3% Cr 1% Mo steel which were gamma-quenched and tempered by the supplier according to established procedures of the manufacturer (oil quench from gamma followed by tempering at 550°C). The treatments were made

in the factory with the typical tolerance of an industrial process. The results of the mechanical tests were within an acceptable range without significant variations among samples. However, the Izod notch toughness (impact test) was not uniform, showing scattered data (20-43 J).

Typical plots of FWHM vs θ are shown in Figure 8 for steels with different Izod notch toughness. A clear gap between the total line breadth functions is evident. From the line broadening analysis it was deduced that the size effect was approximately the same in all samples. STM observations support this finding. Thus, the microstrain was the main reason for the differences in the broadening effect.

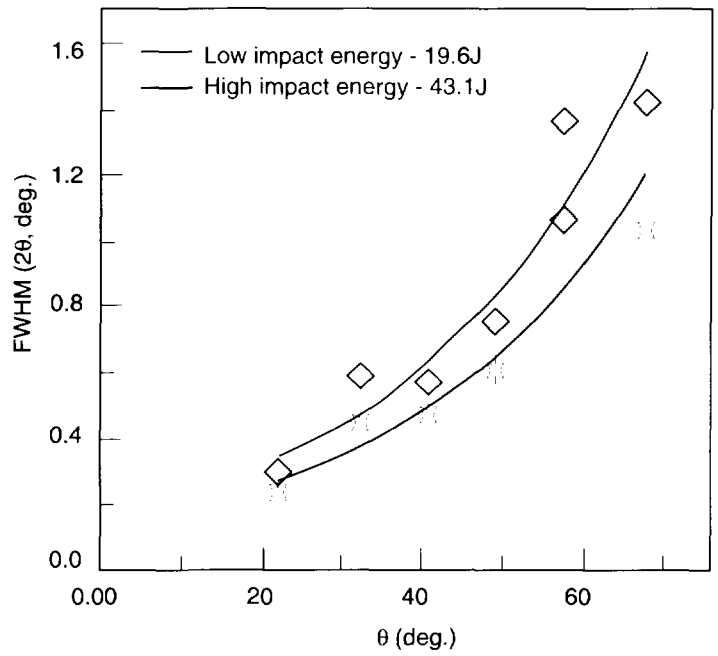

Fig. 8: Line breadth (FWHM) of steels with two different Izod notch toughness.

Figure 9 shows that the microstrain was correlated with the Izod notch toughness, exhibiting linear relation.

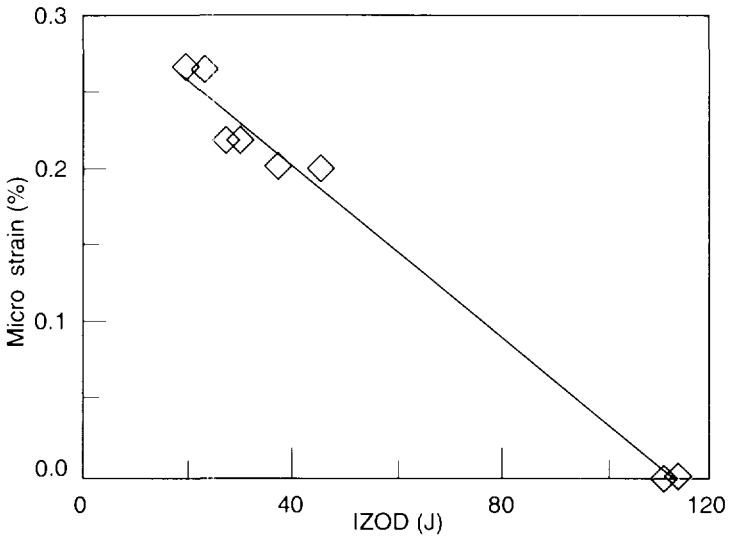

Fig. 9: Correlation between microstrain and Izod impact data for heat resisting steels.

4.2 *Heavily alloyed steel*

The high speed steel M10 is heavily alloyed (0.9% C, 0.3% Mn, 0.3% Si, 4.2% Cr, 8.2% Mo, 2% V, the balance being Fe). The alloy is heterogeneous with two kinds of carbides. An X-ray diffractogram (Fig. 10) shows sharp lines of carbides and broad lines of alpha- Fe. The difference in broadening effects between the metallic phase and carbides is displayed in Figure11.

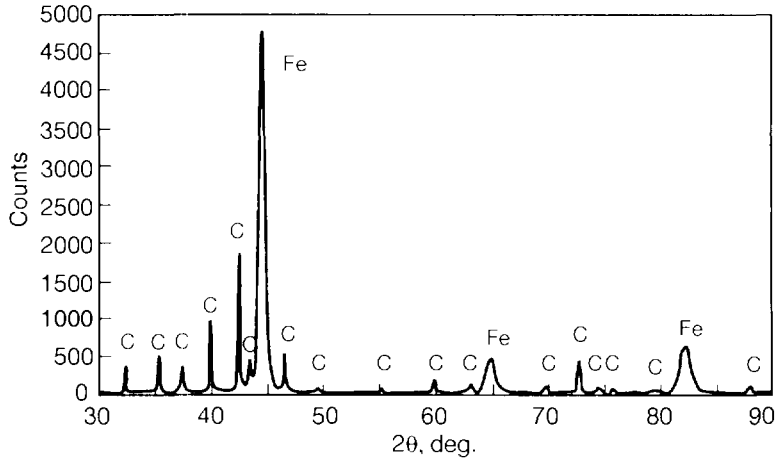

Fig. 10: Diffractograms of high speed steel (M10) after electropolishing (sharp lines for carbides and broad lines for iron base a phase).

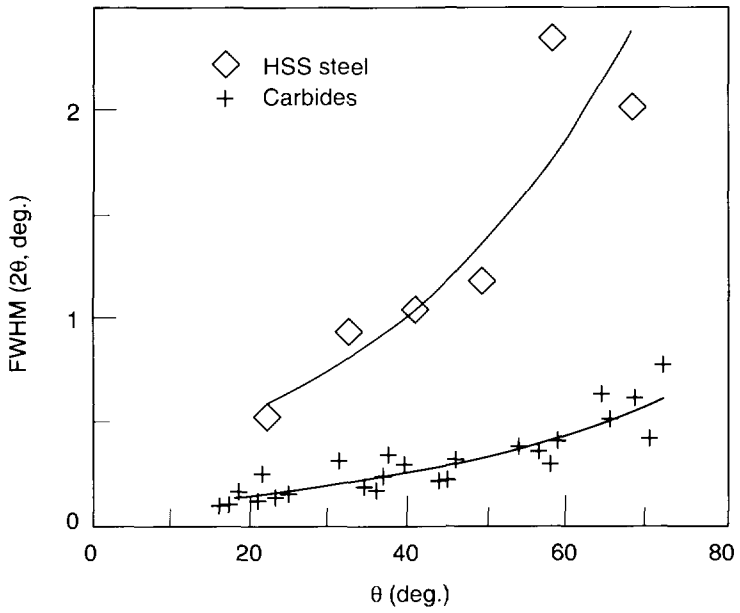

Fig. 11: Line breadth (FWHM) versus Bragg angles for tempered steel: comparison between carbides and iron base a phase

Broadening analysis of the carbides does not show size effect and indicates only a small strain (0.06 %). The broadening effects in the metallic structure are caused by the size of the cells (20 nm) and by the microstrain (0.4%). This value of microstrain exceeds the known elastic/plastic limit. Thus, it is suspected to be a structural broadening effect, like overlapping diffraction lines of two phases with close lattice parameters (like two alpha-like structures of different composition). To check this hypothesis, additional studies using TEM, STM, etc. are needed. The scattering of steel broadening is typical to other steels.

Nonuniform broadening effect in steels

The scattering of FWHM values around the polynomial function (see Fig. 11) is systematic and not random. It may be attributed to tetragonal distortion because the FWHM of *200* and *310* reflections were always higher than the average trend. When the tempering of medium carbon low alloy steel is completed, and all carbon has been segregated, the

broadening becomes uniform and the tetragonality distortion disappears (Fig. 12). However, in the HSS (Fig. 11), in spite of the fact that the alpha Fe phase is mixed with carbides, it still exhibits "tetragonal distortion".

Nonuniform broadening effects were found also in ball-milled iron (Ungár, 1995) and are attributed to the effect of dislocation contrast (Ungár and Borbély, 1996).

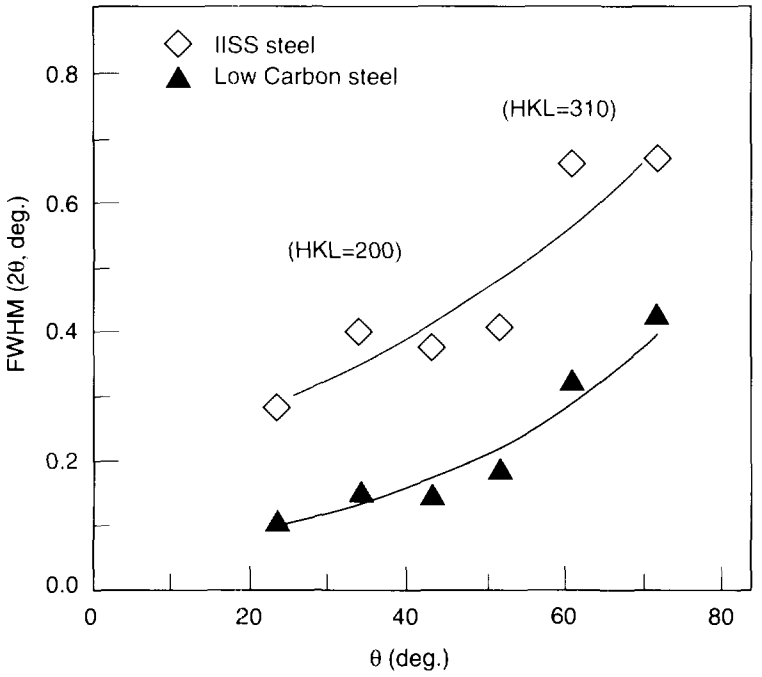

Fig. 12: Line breadth (FWHM) vs Bragg angles for tempered steel: nonuniform broadening effect.

4.3 *Alloying and heat treatments*

Heat treatment of pure uranium- A pure uranium sample containing less than 500 ppm impurities was heat treated at 800°C for 6 hours and quenched in water. Other samples were held at 800°C for 2 h and cooled slowly at the furnace cooling rate. One of these samples was annealed at 200°C for 24 h and cooled slowly. The diffraction patterns of these samples showed that, even in pure uranium, there is a distinguishable line broadening effect after quenching from high temperature (Fig. 13). The sample that was

furnace-cooled gave the sharpest diffraction spectrum available for uranium.

The Williamson-Hall analysis resulted in a rather small microstrain of 0.065% in the water-quenched sample and 0.049% in the slowly cooled sample (see Table 2), both from the same temperature (800°C). Considering the variation between thermal expansion coefficients in different directions in uranium as 15 ppm/K, thermal strain due to of anisotropic contraction can be built up by cooling from 320 to 440°C. According to Collot and Reisse (1971), it is reasonable to assume that only above 420°C plastic deformation relax all thermal stresses instantly. Thus, it is concluded that uranium samples quenched from high temperatures should include residual microstrain up to 0.065%, probably due to thermal stresses.

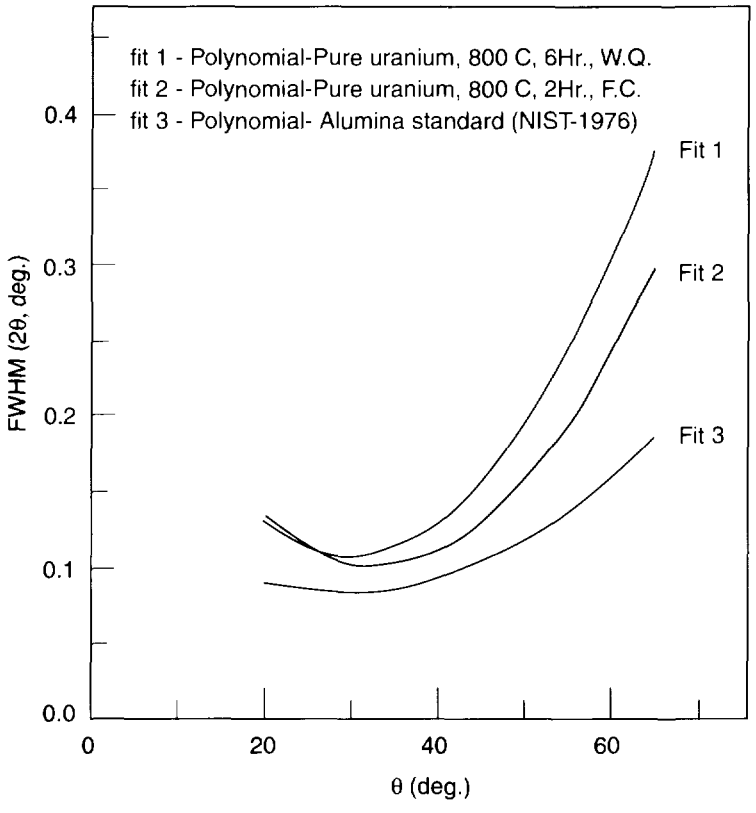

Fig. 13: Broadening effects in pure U after heat treatment at 800°C for 6 h and water quench (Fit 1) and, after slowly cooling from 800°C to room temperature at the furnace cooling rate (Fit 2). (Both samples were polished electrolytically).

Table 2: Microstrain after several heat treatments

Sample	Heat treatment	Microstrain (%)
pure uranium	800°C, 2h, F.C.	0.049
pure uranium	800°C, 6h, W.Q.	0.064
U - 0.2 wt.% V	850°C, 2h, F.C.	0.063
U - 0.2 wt.% V	850°C, 2h, W.Q.	0.171

FC - Furnace Cooling
WQ - Water Guenching

Microstrain in heat-treated dilute uranium-Ta and W alloys - Tungsten and tantalum were reported to be immiscible in α uranium and to have small solubility in γ uranium. We observed that quenching of uranium with small amounts of Ta and W from temperatures in the γ range produces very small lattice distortion; however, severe broadening effects occur (Fig. 14). Williamson-Hall analysis resulted in a pure strain effect (no small domains), which increases with the concentration of the supersaturated alloy.

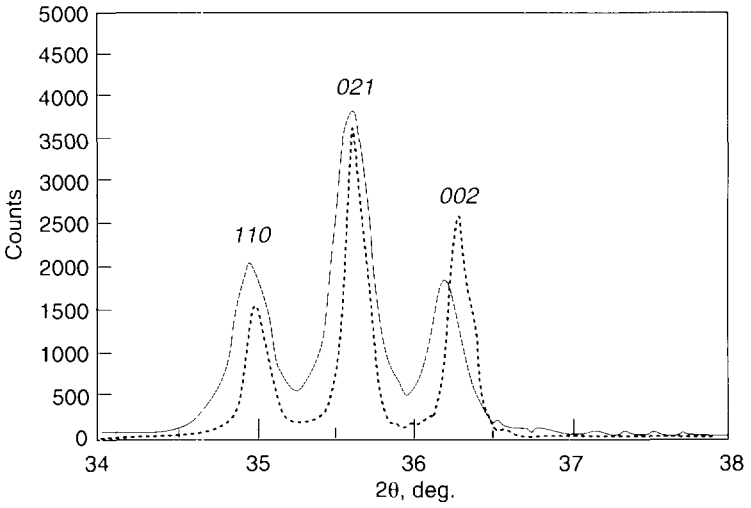

Fig. 14: Part of the U-Ta spectrum after water- quenching( ) and after slow cooling (---) from 1040°C, showing severe broadening effect in the sample after γ quenching.

A plot of microstrain vs concentration is presended in Figure 15 for both alloying elements W and Ta. It should be noted that the solubility limit was defined by the appearance

of the *cI2* structure diffraction lines for W and Ta, as well as by SEM observations. We found that the solubility limits for the alloys are 2.6 and 2.00 at.% for Ta and W, respectively. These values are above the reported data for the solubility limits in γ uranium (Schramm et al., 1950), but are beyond the solubility limit of these elements in α-uranium. Therefore, in both cases the supersaturated state should be assumed.

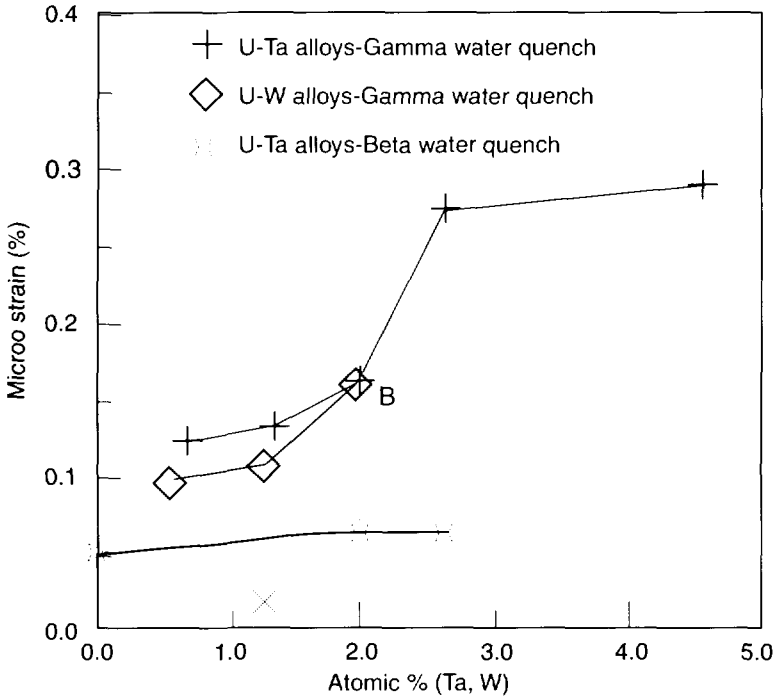

Fig. 15: Microstrain vs concentration in quenched samples of U with Ta and W after g quenching, and with Ta after b quenching.

Quenching from the β phase resulted in different behavior of W and Ta. Tungsten was found to be a β stabilizer. The characteristic of the room temperature β structure of U dilute W is reported elsewhere (Dayan et al., 1994). On the other hand, all samples with Ta quenched from β showed diffraction of free tantalum, without any broadening effect (Dayan and Kimmel, 1996). The microstrain of β-quenched samples is displayed in Figure15, which shws that the strain in β–quenched samples is in the range of

4.4 Microstrain and mechanical properties

thermal stress and independent of Ta concentration.

Effects of cold work - Cold work of uranium (U-0.2% V) results in increased hardness. The hardness increases sharply until 10% reduction and continues to rise moderately but steadily. XRD studies of forged samples showed a broadening effect which can be removed by thermal annealing. After data processing by the Williamson-Hall method, the strain component was found to increase with the percent reduction in the same manner as the hardness. The simultaneous increase of both characteristics, the microstrain and the hardness, is illustrated in Figure 16. The correlation between degree of cold work and XRD line broadening has been reported in other alloys, for example in carbon steel (Kurita, 1991) and in Al-Mg (Ji et al., 1993).

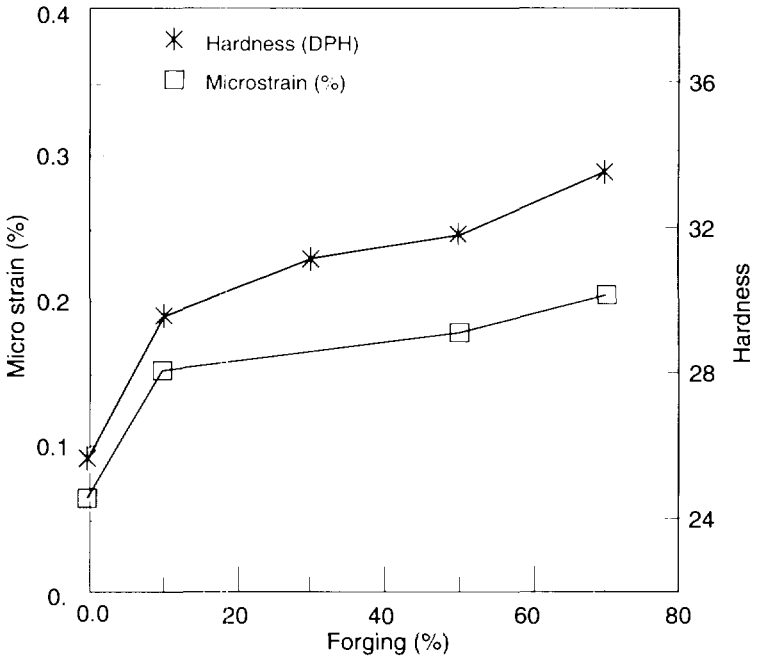

Fig. 16: Simultaneous increase of microstrain and hardness in forged U 0.2 wt.% V.

Fracture toughness - The correlation between XRD line width and fracture toughness of U-0.75wt.% Ti samples was evaluated. The samples underwent the same heat treatments, solution treatment at 850°C for 20 min and water quench, following aging at 370°C for 6 h, and displayed almost the same mechanical properties such as tensile strength, elongation and hardness, within an acceptable range of tolerance. However, the fracture toughness (FT) results were scattered within a wide range of values. After performing XRD line broadening analysis, it was found that the domain size was the same for all samples, but the microstrain was fluctuating. Figure 17 shows that microstrain and fracture toughness are linearly dependent.

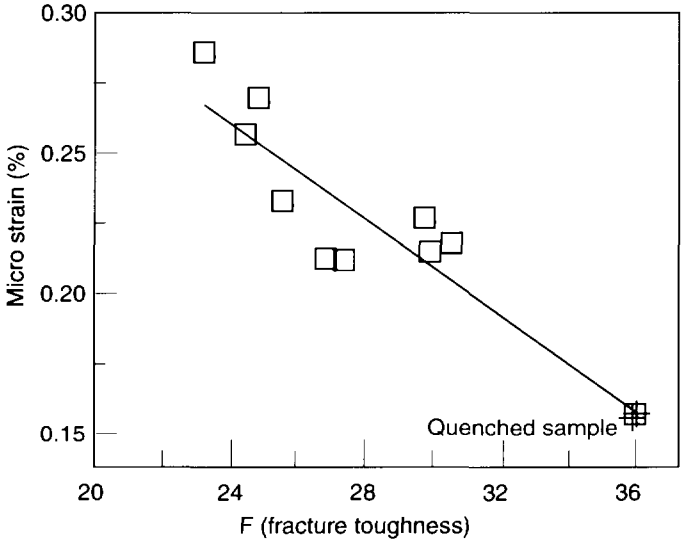

Fig. 17: Correlation between microstrain and fracture toughness (stress intensity factor), expressed in KSI√in.

Effect of solubility - Since a correlation was found between solid solution and microstrain, we deemed, it worthwhile to check the hardness of each sample with a metastable solid solution. The results show a simultaneous increase of hardness with microstrain for U-Ta alloys (Fig. 18).

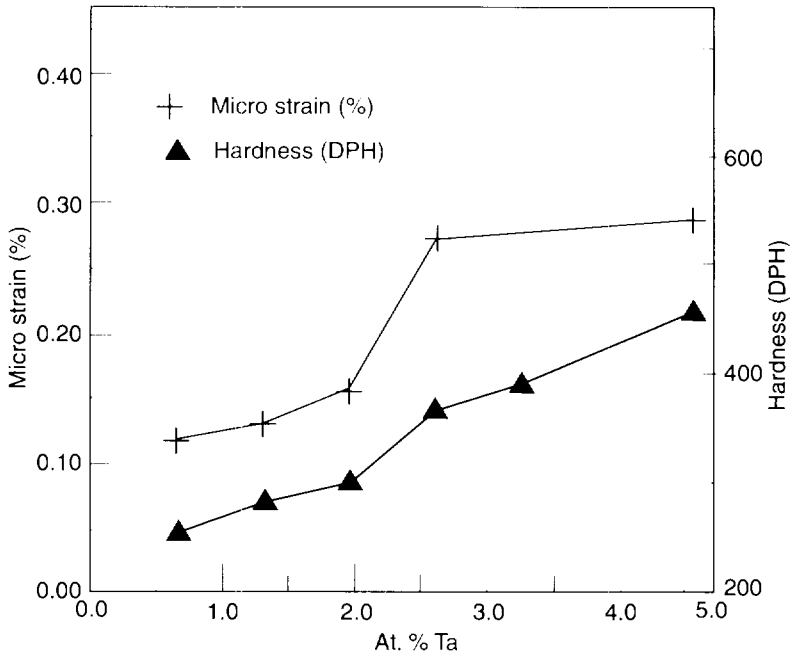

Fig. 18: Simultaneous increase of microstrain and hardness in alloyed U-Ta as a tool for determining solubility limit.

5. Summary and Discussion

The observations made in the two different system studied were similar.

1. A surface free of polishing damage is required and electropolishing is an efficient way to remove surface damage in uranium alloys and in steels.

2. The strain is the main probe for a physical process in the metallic systems. Metastable solid solutions in metallic alloys increase the microstrain.

3. The microstrain is probably correlated with fracture toughness as indicated in Figure 17. Such correlation may be of scientific significance because it provides a convenient way to study the empirical connection between these two properties. Furthermore, it is readily seen from Figure 8 that if the microstrain is really a linear function of the Izod notch toughness, one can evaluate the upper limit of Izod notch toughness for the heat-resisting steels (by extrapolation to the point with zero microstrain). The value of 114 J which was derived by such a procedure is in agreement with the high values of Izod notch toughness in steels (Wyatt and Dew-Huges, 1974). If this correlation will be established with more data and also with fracture toughness tests, it could become an excellent characterization tool for both quality

control and research.

4. The correlation between microstrain and hardness or strength is not absolutely clear. In several cases, for example U-Ta dilute alloys, aging raised the hardness and relaxed the microstrain. In heat-resisting steels the variations in hardness and strength were equal for some samples, but the microsrain differed. This point is important because there is also no general rule which correlates hardness with toughness. Broadening analysis can be used as an additional tool to clarify this point.

This work showed that a considerable amount of information relevant to the tested materials structure can be obtained from an analysis of the broadening effects. In spite of the fact that X-rays are mainly a near-surface probe, in particular for uranium, most artifacts caused by improper surface preparation can be eliminated.

Two different types of broadening effects were found: those caused by cold work and those observed in metastable solid solutions. In both cases the broadening effect could be quantified using in, microstrain as the parameter in the analysis. A correlation we found between the strain, the amount of cold work, and the amount of an added element

For materials belonging to a similar family and when the effect of concentration was eliminated, we were able to obtain a general experimental dependence between the microstrain and the hardness of the samples. In cases of softening or hardening (by thermal annealing, aging or cold work) we could replace the hardness test could be replaced by measurement of microstrain. Nevertheless, we do not claim that this dependence is a general rule; it should be utilized only after making a calibration curve.

It is possible that the microstrain following cold work has a different origin from that which is induced by metastable supersaturated solid solution. Whereas in the case of cold work we obtained both strain and size effects, in the supersaturated state we found mostly microstrain. We tend to attribute this microstrain to fluctuations in concentration of the added alloying element. These fluctuations in concentration result in an enhanced hardening.

The main effect of adding new elements into solid solution is the lattice parameter distortion, which results in shifts of the XRD line positions. In uranium the solubility limit of most elements is less than 1% at., with almost no change in lattice parameters. However, metastable supersaturated α' uranium alloys with solubility up to 5 at.%. are known in uranium with added γ-stabilizing lements, titanium, niobium, zirconium, molybdenum, ruthenium and rhenium. (Douglas 1961; Tangri, K. and Williams 1961; Virot 1962, Hills et al., 1963; 1965; Jackson et al., 1963; Anagnostides et al., 1964; Tangri, et al., 1965; Jackson and Larsen, 1967; Yakel 1976). Continuous change of lattice parameters of α' uranium alloys was reported by many workers. Together with peaks shifts, severe line broadening was also reported (Douglas, 1961), but without quantitative data. TEM studies of γ water quenched uranium with additions Ti and Ti+V exhibited nonhomogeneous structures within the nano-scale (Landau et al., 1986, 1993). Therefore, it is reasonable to attribute the microstrain found by XRD to local fluctuations in the concentrations of the alloying elements.

Whereas the stability range of the γ stabilizer elements (Nb, Zr, Ti, Mo etc.) is very large in the γ phase, in U-Ta and U-W the solubility in γ is limited to less than 3 at.%. Consequently, the α structure lattice parameters in γ quenched samples with Ta and W are almost unmodified (Dayan et al., 1994; Dayan and Kimmel, 1996). However, broadening effects in the α structure in γ quenched samples were quite obvious, and line broadening analysis was the most sensitive method for the characterization of alloys which are not defined as γ stabilizers, such as U-Ta , U-W and U-V. The correlation between microstrain and concentration of the dissolved element can be used to measure the solubility limit in the high-temperature phase. In the range where the microstrain was increasing continuously with concentration after quenching from the high-temperature phase, it is implied that during the solution treatment at the higher temperature, the equilibrium state was a solid solution. The solubility limit of Ta in γ - U is indicated by the "saturation" of the broadening effect as a function of (see Fig. 18). The minor difference in the microstrain values of pure U in comparison with U-0.2%wt. V after complete annealing (see Table 1), may be attributed to an excess of vanadium which could not be removed completely.

6. References

Anagnostidis, M., Colombie, M. and Monti, H. (1964) J. Nucl. Mat. 11:67-76.

Burke, J.J., Colling, D.A., Gorum, A.E. and Greenspan, J. Physical Metallurgy of Uranium Alloys., Brook Hill Co., Chestnut Hill, Massachusetts, in cooperation with the Metals and Ceramics Information Center, Columbus, Ohio, 1976.

Chiotti, P., Klepfer, H.H. and White, R.W. (1959) Trans. Am. Soc. Metals 51: 772.

Collot, C. and Reisse, R. (1971) Mem. Sci. Rev. Met. 6:419-434.

Dayan, D., Beeri, O., Herrmann, B., Landau, A., Zahavi, A. Livne, Z. And Kimmel, G. (1994) J. Alloys Compounds 226:89-93.

Dayan, D. and Kimmel, G.(1996) J. Alloys Compounds 243:161-166.

Douglas, D. L. (1961) Trans. ASM 53:307-319.

Guillou, N., Auffredic, J.P. and Louer, D. (1995) Powd. Diffr. 10:236-240.

Gupta, R.K. and Anantharaman, T.R. (1971) Z. Metallkd. 62:732-735.

Halder, N.C. and Wagner, C.N.J. (1996) Adv. X-Ray Anal. 9:91-102.

Jackson, R. L., and Larsen, W. L. (1967) J. Nucl. Mat. 21: 263-276.

Jackson, R. J., Williams, D. E. and Larsen, W. L (1963) J. Less Comm. Met. 5:443-461.

Ji, N., Lebrun, J.L. and Sainfort, P.(1993) Mater. Sci. Forum 133-136:537-542.

Hills, R. F.,Howlett B. W., and Butcher, B. R. (1965) J. Nucl. Mat. 16:109-128.

Kimmel, G. and Dayan, D. (1995) Proceeding International Conference, X-Ray Powder Diffraction, Analysis of Real Structure of Matter, Size and Strain, 95 21-25 Aug. 1995, Liptovsky Mikulás, Slovakia, I20, p. 23.

Klug, H. P. and Alexander L. E. (1974) X-Ray Diffraction Procedures 2nd. ed. John Wiley and Sons, New York.

Kurita, M. (1991) Adv. in X-ray Anal. 34:633-642.

Landau, A., Kimmel, G. and Talianker, M. (1986) Script. Met. 20:1313-1316.

Landau, A. Talianker, M. and Kimmel, G. (1993) J. Nucl. Mat. 207:274-279.

Langford J.I. (1992) Accuracy in Powder Diffraction II, E. Prince and J.K. Stalick (eds) NIST 846, 110-126.

Langford, J.I, Boultif, A., Auffrédic, J.P. and Louër, D.(1993) J. Appl. Cryst. 26:22-33.

Langford, J.I., Delhez, R., de Keijser, Th. H. and Mittemeijer, E.J.(1988) Aust. J. Phys. 41:173-187.

Langford, J.I, Louër, D., Sonnenveld, E.J. and Visser, J.W.(1986) Powder Diffraction 1:211-221.

Louër, D. (1994) Adv. X-ray Anal. 37: 27-35.

Nandi, R. K. and Sen Gupta, S. P. (1978) J. Appl. Cryst. 11: 6-9.

Saller, H.A. and Rough, F. A. (1952) U. S. A.E.C. publ., AECD-3323 and BMI-716.

Scherrer, P. (1918) Goettingen. Nach. 2:98.

Schramm, F. G., Gordon, R. and Kaufman, A. R. (1950) J. Metals 188:195.

Stokes, A.R. and Wilson, A.J.C. (1944) Proc. Pys. Soc. Lond. 56:174-181.

Tangri, K. and Williams, G. I. (1961) J. Nucl. Mat. 4:226-233.

Tangri, K., Chaudhuri, D. K. and Rao, C. N. (1965) J. Nucl. Mat. 15:228-287.

Ungár, T. (1995) Proceeding International Conference, X-Ray Powder Diffraction, Analysis of Real Structure of Matter, Size and Strain, 95 21-25 Aug. 1995, Liptovsky Mikulás, Slovakia, I12, p. 23.

Ungár, T. and Borbély, A. (1996) Appl. Phys. Lett. 69:3173-3175.

Virot, A. (1962) J. Nucl. Mat. 5: 109-119.

Wagner, C.N.J. and Aqua, E.N. (1963) Adv. X-ray Anal. 7:46-64.

Williamson, G.K. and Hall, W.M. (1953) Acta Met. 1:22-31.

Wilson, A.J.W. (1962) X-Ray Optics, Methuen, London.

Wyatt O.H., and Dew-Huges, D. (1974) Metals, Ceramic and Polymers, Cambridge University Press, London.

Yakel, H. L. (1976) "Review of X-ray Diffraction Studies in Uranium Alloys. Physical Metallurgy of Uranium Alloys. Burke, J.B. Colling, D.A. Gorum A.E., and Greenspan, J. [Eds.]Chapt 7. Pp. 259-308 Brook Hill Publishing Company, Chestnut Hill, MA, U.S.A.